X-ray diffraction, microstructure, Mössbauer and magnetization studies of nanostructured Fe50Ni50 alloy prepared by mechanical alloying

Abderrahim Guittoum, Abdelhamid Layadi, Abdelkader Bourzami, H Tafat, Nassim Souami, Slimane Boutarfaia, Daniel Lacour

X-ray diffraction, microstructure, Mössbauer and magnetization studies of nanostructured $Fe_{50}Ni_{50}$ alloy prepared by mechanical alloying

A. Guittoum[a,*], A. Layadi[b], A. Bourzami[b], H. Tafat[c], N. Souami[a], S. Boutarfaia[d], D. Lacour[e]

[a]*Nuclear Research Center of Algiers, 2 Bd Frantz Fanon, BP 399, Alger-Gare, Alger, Algeria*
[b]*Département de Physique, Faculté des Sciences, Université de Sétif 19000, Algeria*
[c]*Laboratory S.G.M., UST.H.B., BP 32, Bab-Ezzouar, Algeria*
[d]*Centre de Recherche Nucléaire de Draria, BP 43, Alger, Algeria*
[e]*LPM, Nancy-University, CNRS, 54506 Vandoeuvre les Nancy, France*

Nanocrystalline $Fe_{50}Ni_{50}$ alloy samples were prepared by the mechanical alloying process using planetary high-energy ball mill. The alloy formation and different physical properties were investigated as a function of milling time, t, (in the 0–50 h range) by means of the X-ray diffraction (XRD) technique, scanning electron microscopy (SEM), energy dispersive X-ray (EDAX), Mo¨ssbauer spectroscopy and the vibrating sample magnetometer (VSM). The complete formation of γ-FeNi is observed after 24 h milling. When milling time increases from 0 to 50 h, the lattice parameter increases towards the $Fe_{50}Ni_{50}$ bulk value, the grain size decreases from 67 to 13 nm, while the strain increases from 0.09% to 0.41%. Grain morphologies at different formation stages were observed by SEM. Saturation magnetization and coercive fields derived from the hysteresis curves are discussed as a function of milling time.

Keywords: FeNi alloy; X-ray diffraction; Microscopy; Mössbauer effect; Magnetic measurement

1. Introduction

Nanomaterials are experiencing a rapid development in recent years due to their potential applications in a wide variety of technological areas such as magnetic data storage, electronics, catalysis, ceramics and structural components, etc. [1]. Recently, nanocrystalline magnetic materials have been intensively investigated because of their remarkable properties such as saturation magnetization, coercivity, magnetic ordering temperature and hyperfine magnetic field which significantly differ from those of microcrystalline materials and are sensitive to the structure and microstructure [2]. FeNi alloys are industrially used for high-saturation magnetization and low-coercivity applications. The benefits found in these magnetic nanostructured alloys stem from their chemical and structural properties which are important for the magnetic properties [3]. Also, such materials are of interest for magnetic research since the reduction of grain sizes to single magnetic domain sizes offers the possibility to eliminate the influence from magnetic walls [4].

Several methods including thermal evaporation [5], electrodeposition [6], gas condensation [7], rapid solidification [8] and metal plasma reaction [9] were used to prepare nanostructured FeNi materials. Among these methods, mechanical alloying (MA) is a powerful technique which allows the preparation of nanostructured FeNi alloys [10–12].

The present work deals with the preparation of nanocrystalline $Fe_{50}Ni_{50}$ compound by high-energy alloying technique. X-ray diffraction (XRD), Mössbauer studies and magnetic measurements are used for a better understanding of the evolution of $Fe_{50}Ni_{50}$ phase during the

*Corresponding author.
E-mail address: guittoum@yahoo.fr (A. Guittoum).

elaboration. Scanning electron microscopy (SEM) and X-ray microanalysis are also used to study the morphology of the powder and to investigate the chemical homogeneity of the powder particles.

2. Experiments

Elemental Fe and Ni powders of 99.9% purity and particle sizes smaller than 100 μm were separately weighted and mixed to get the desired composition. The mechanical alloying process was performed in a planetary high-energy ball mill (Retch PM400). To prevent oxidation phenomena, the mixed powder was sealed in a cylindrical vial under argon atmosphere with stainless steel balls. The ball-to-powder weight ratio was 15:1. The vial rotation speed was equal to 180 tr/min. Different milling times ranging from 2 to 50 h were used. To avoid excessive heating during milling, each 15 min of milling was followed by a pause of 15 min under Ar atmosphere. XRD experiments were performed with a Philips X-Pert Pro diffractometer in continuous scanning mode using Cu Kα radiation. X-ray patterns were analyzed by Winfit software [13] based on the Warren and Averbach method [14]. This method allows us to calculate the average grain size together with the mean level of internal strain. Before doing this, the Cu $K\alpha_2$ radiation was analytically suppressed from the profiles using the Rachinger method of X-Pert plus software. SEM and X-ray microanalysis studies were performed on a Philips XL 30 microscope coupled to an energy dispersive analyzer (EDX). Mössbauer spectra were obtained at room temperature with a Wissel instrument in the constant acceleration mode, using a radioactive ^{57}Co source diffused into a Rhodium matrix. Metallic iron was used for energy calibration and also as a reference for isomer shift. Mössbauer spectra were evaluated with the Recoil software using the Voigt-based hyperfine field distribution method (HFD-VB-F) [15].

Hysteresis curves were obtained at room temperature using a vibrating sample magnetometer (VSM) with the external magnetic field H in the 0–10 kOe range.

3. Results

3.1. Structure

XRD measurements were performed for all mixed powders at different milling times. The obtained diffraction patterns allowed us to follow the process of alloy formation.

Fig. 1 shows the evolution of XRD patterns for $Fe_{50}Ni_{50}$ samples as a function of milling time. XRD spectrum for the starting powder (labeled 0 h in Fig. 1) shows the reflections corresponding to distinct bcc Fe and fcc Ni metals. One can clearly observes that the diffraction peaks broaden with increasing milling time indicating a continuous decrease in the grain sizes and the introduction of lattice strain. This broadening is due to the second-order

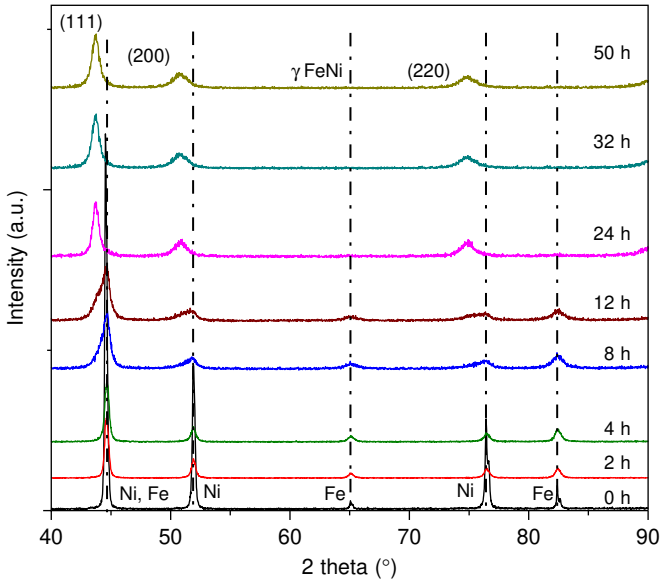

Fig. 1. X-ray diffraction spectra of mechanical alloying $Fe_{50}Ni_{50}$ for various milling times.

internal stress which acts as a macroscopic level of the crystallites and produces a broadening of X-ray peaks [16].

After 24 h of milling, we observed that the reflection peaks (2 0 0) and (2 1 1) corresponding to α-Fe bcc disappear and the Ni peaks slightly shift towards lower angles. This proves that Fe atoms dissolve in the Nickel lattice leading to the formation of fcc solid solution γ (Fe–Ni) (called taenite) with space group Fm3m. The slightly angular shift is attributed to the formation of taenite phase and also to the first-order internal stress induced by milling. The first-order angular stress acts as a macroscopic level by modifying the lattice parameter and consequently produces an angular shift of XRD peaks [16]. It is worth noting that for $Fe_{50}Ni_{50}$ obtained by mechanical alloying, the formation of fcc solid solution γ (Fe−Ni) (i.e., taenite) was confirmed by Jartych et al. [17] after 50 h of milling time, Kaloshkin et al. [18] and Baldokhin et al. [19] after 1 h of milling.

Fig. 2 presents the change of lattice parameter (a) vs milling time for $Fe_{50}Ni_{50}$ samples. The lattice parameter monotonously increases with milling time from 0.35208 ± 0.00005 nm for a pure Ni to 0.35953 ± 0.00005 nm for 50 h of milling. We observe an abrupt increase of the lattice parameter when t is increased from 8 to 12 h (see Fig. 2), recall that in this range, $Fe_{50}Ni_{50}$ starts progressively to form while pure Fe disappears; between 24 and 50 h (where only the alloy phase exists), the increase in lattice parameter is not as large as in the previous stage. For the longest milling time, the lattice parameter value is very close to the $Fe_{50}Ni_{50}$ bulk value of 0.35975 nm. The increase of lattice parameter with milling time is due to the disordering of the alloy as was suggested by Oleszak and Shingu [20] in the case of FeAl alloy. It is interesting to note, for comparison, that for mechanical alloying $Fe_{50}Ni_{50}$, Jartych et al. [17] found a lattice parameter

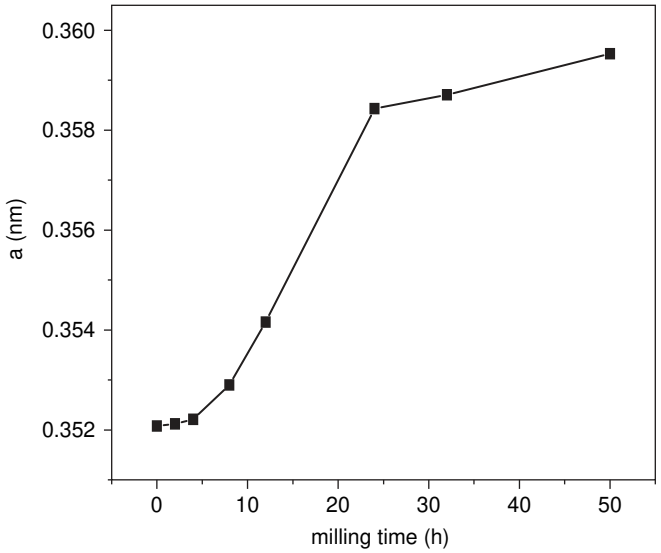

Fig. 2. Lattice parameter a (nm) versus milling time for $Fe_{50}Ni_{50}$ samples.

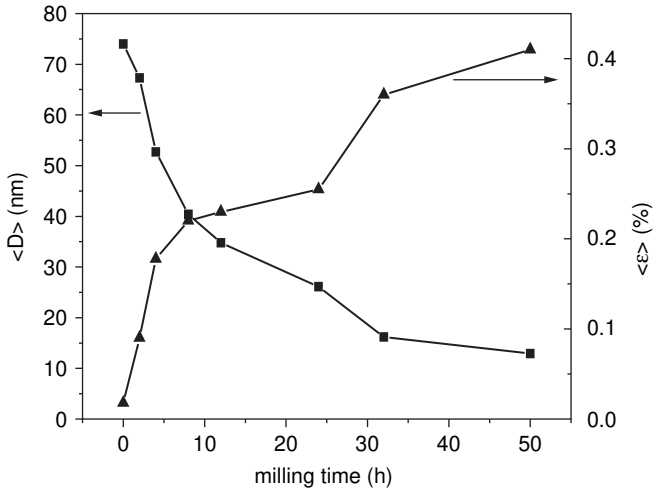

Fig. 3. Average crystallite sizes $\langle D \rangle$ (nm) and mean internal strain $\langle \varepsilon \rangle$ (%) of $Fe_{50}Ni_{50}$ versus milling time.

equal to 0.3594 nm after 50 h of milling using a planetary ball mill and Tcherdyntsev et al. [12] obtained a value of 0.3590 nm after 1 h of milling with a planetary ball mill. Djekoun et al. [21] achieved a lattice parameter value of 0.3601 nm after 322 h of milling using Fritsh Pulverisette 7 planetary ball mill.

Fig. 3 presents the evolution of the average crystallite sizes $\langle D \rangle$ and the mean level of internal strains $\langle \varepsilon \rangle$ as a function of milling time. It is clear that the crystallite size monotonously decreases with increasing milling time. This decrease in $\langle D \rangle$ is accompanied by an increase of the mean internal strain level $\langle \varepsilon \rangle$. Similar dependencies of D and ε parameters on milling time were reported by Djekoun et al. [21] for mechanically alloyed $Fe_{50}Ni_{50}$ compound and also by Hamzaoui et al. [22] for $Fe_{80}Ni_{20}$ elaborated by high-energy ball milling. The $\langle D \rangle$ values of the crystallite sizes decreases from $\langle D \rangle = 67.3 \pm 2$ nm for the 2 h milled powder to 12.9 ± 2 nm for a milling time of 50 h and the mean internal strain $\langle \varepsilon \rangle$ values increases from $\langle \varepsilon \rangle = 0.09 \pm 0.05\%$ to $0.41 \pm 0.05\%$. We would like to emphasize that for the unmilled powder, the value of the crystallite size equal to 74 nm and the internal strain of 0.018% are only given by the instrumental width of the XRD peaks. It is interesting to note that Jartych et al. [17] obtained a crystallite size and lattice strain of 10 nm and 0.5% after 50 h of milling using a high-energy planetary ball mill and Djekoun et al. [23] achieved a grain size value of 8 nm after 48 h of milling using Pulverisette 7 planetary ball mill. Also note that the grain size and strain values found in this work (12.9 nm and 0.41%) are comparable to those reported by Pękala et al. [24] (14 nm and 0.5%) but after 400 h of milling using low-energy horizontal ball mill. Also, Lima et al. [25] obtained a crystallite size of 15 nm for nanostructured $Fe_{50}Ni_{50}$ alloy prepared by chemical reduction.

3.2. Microstructure

The powder morphology was studied by SEM. Fig. 4 shows the morphological evolution of $Fe_{50}Ni_{50}$ alloy as a function of milling time (0, 2, 4, 8, 24 and 50 h). It can be seen that different morphologies are present during the mechanical alloying stages. For the unmilled powder (Fig. 4a), the existence of iron particles (the larger ones) and Ni particles (smaller ones) are clearly observed. As a result of intensive fracture and cold welding as presented in Fig. 4b and c, composites particles are formed after 2 h of milling time. For 4 h of milling time, the particles change into a flake or platelet shape (Fig. 4d). Some of these particles present a layered structure formed of superposed Ni and Fe layers (Fig. 4e), typical of materials prepared by mechanical alloying for ductile or brittle elements as indicated by Davis et al. [26] and Otmani et al. [27]. This layered structure is gradually destroyed with increasing milling time. With milling time greater than 4 h, one can see that there is a stage where the formation of flake shape particles is favored; the example shown here is for 8 h of milling time (Fig. 4f) and a stage where the platelet shape particles dominate for example for 24 h of milling (see Fig. 4g). By increasing the milling time, the mechanical alloying progress and the refinement of particles size continues. For the longest milling time (50 h; see Fig. 4h), the majority of particle grains exhibit a round shape with small diameter; however, one can still note the presence of some big ones having a platelet shape.

Elemental mapping by EDX coupled to the SEM was carried out on the mechanically alloyed powders. Fig. 5 shows the maps of Ni and Fe distribution for the selected areas of some samples. For the short milling times, i.e., for 4 h (Fig. 5a), it is clearly shown that the iron and nickel particles are still separated from each other.

With increasing milling times and for milling time of 12 h (Fig. 5b), it becomes difficult to distinguish between Ni and Fe particles; this indicated the beginning of Ni and Fe alloying process; however, elemental Ni and Fe are still

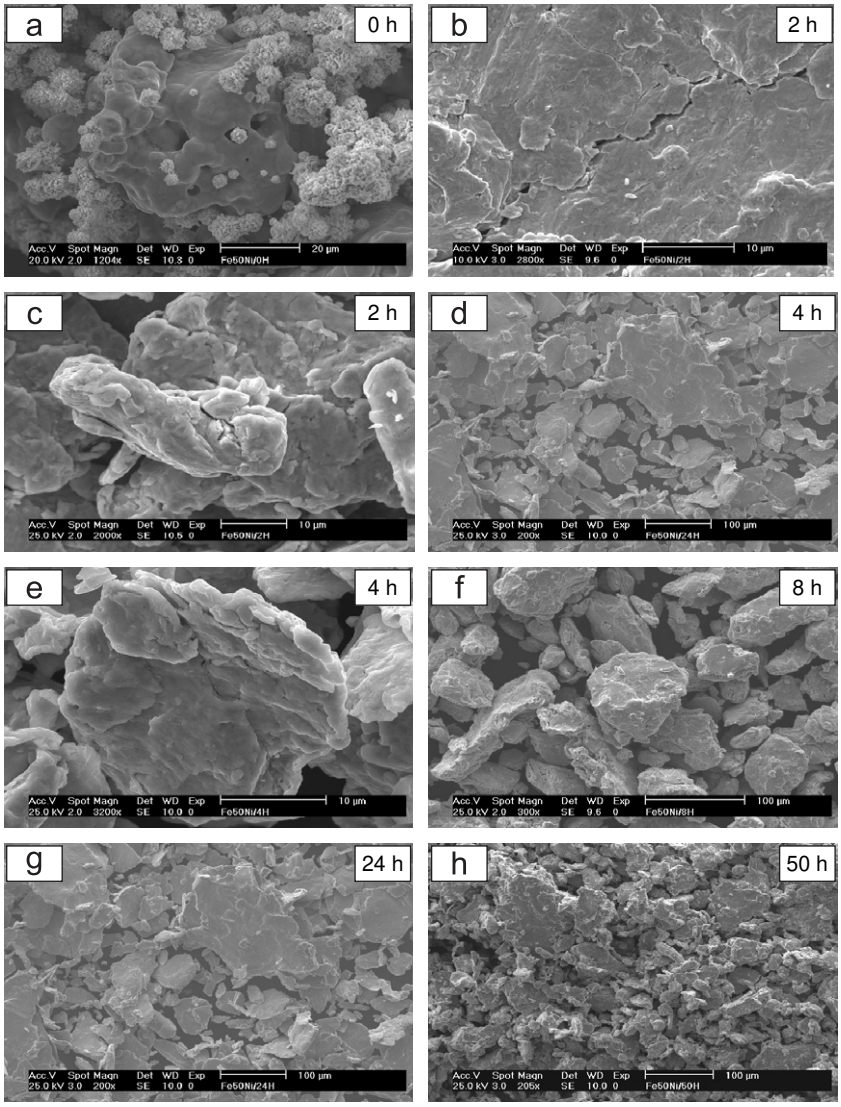

Fig. 4. SEM micrographs of $Fe_{50}Ni_{50}$ powders for various milling times: (a) 0 h (unmilled $Fe_{50}Ni_{50}$), (b, c) 2 h, (d, e) 4 h, (f) 8 h, (g) 24 h and (h) 50 h.

observed. For milling times of 24 h (Fig. 5c) and 50 h (Fig. 5d), the elemental maps indicate that the Fe and Ni elemental distributions are closely correlated, in the error limits of this method, indicating that the two elements are completely alloyed and the NiFe solid solution is formed. These results are very consistent with the XRD analysis (see Section 3.1).

Energy dispersive X-ray (EDAX) analyses were made on all samples. We noted that no Cr contamination from the milling media was observed. Also, no contamination with O_2 was found for all milling times in the error limits of this method.

3.3. Mössbauer spectroscopy

The Mössbauer measurements were done in order to monitor the process of alloy formation at every stage of milling. The room temperature Mössbauer spectra and their corresponding HFD for different milling times are shown in Fig. 6. For the unmilled sample, the spectrum shows the presence of a typical sextet with a mean hyperfine field $\langle H_{hf} \rangle$ equal to 32.98 T which corresponds to the α-Fe present in the starting FeNi powder. The half-width at half-maximum (HWHM) of spectral lines were about 0.12 mm/s. After milling times of 2 and 4 h, the spectra are still characteristic for α-Fe, i.e, magnetically split patterns with six lines. The two spectra were fitted by one sextet with $\langle H_{hf} \rangle = 32.98$ T. The HWHM of spectral lines were about 0.1301 mm/s. For samples milled at 8 and 12 h, it can be seen that the shape of the spectra begin to change with a broadening of the spectral lines in relation to α-iron. For these samples, the Mössbauer spectra were fitted with two sextets for 8 h (not shown here) and two sextets and a singlet line for 12 h milled sample (see Fig. 6). The first sextet originates from of α-Fe with a mean hyperfine field $\langle H_{hf} \rangle = 32.985(41)$ and 32.590(17) T for samples milled at 8 and 12 h, respectively. The second sextet with $\langle H_{hf} \rangle = 30.5(13)$ T (intensity of 26.1%) for 8 h

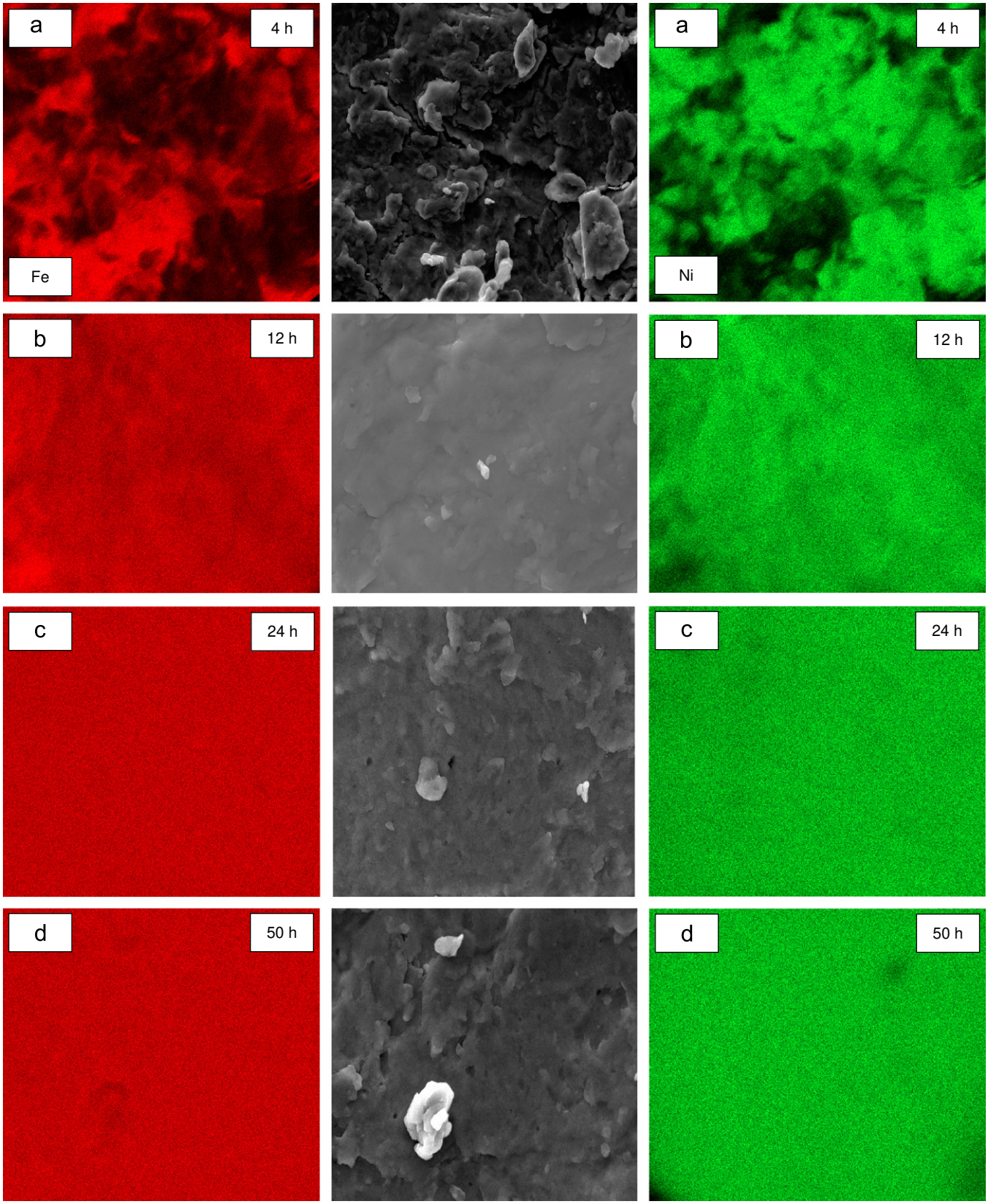

Fig. 5. Maps of Ni and Fe distributions for different milling times: (a) 4 h, (b) 12 h, (c) 24 h and (d) 50 h.

and $\langle H_{hf} \rangle = 29.41(36)$ T (intensity of 32.7%) for 12 h is due to the newly magnetic phase atomically disordered with a composition $\approx Fe_{50}Ni_{50}$ [28,29]. The singlet line is attributed to a fcc iron rich paramagnetic phase that usually coexists with the ferromagnetic fcc around 50% Fe as explained by Lima et al. [25], Scorzelli and Danon [29]

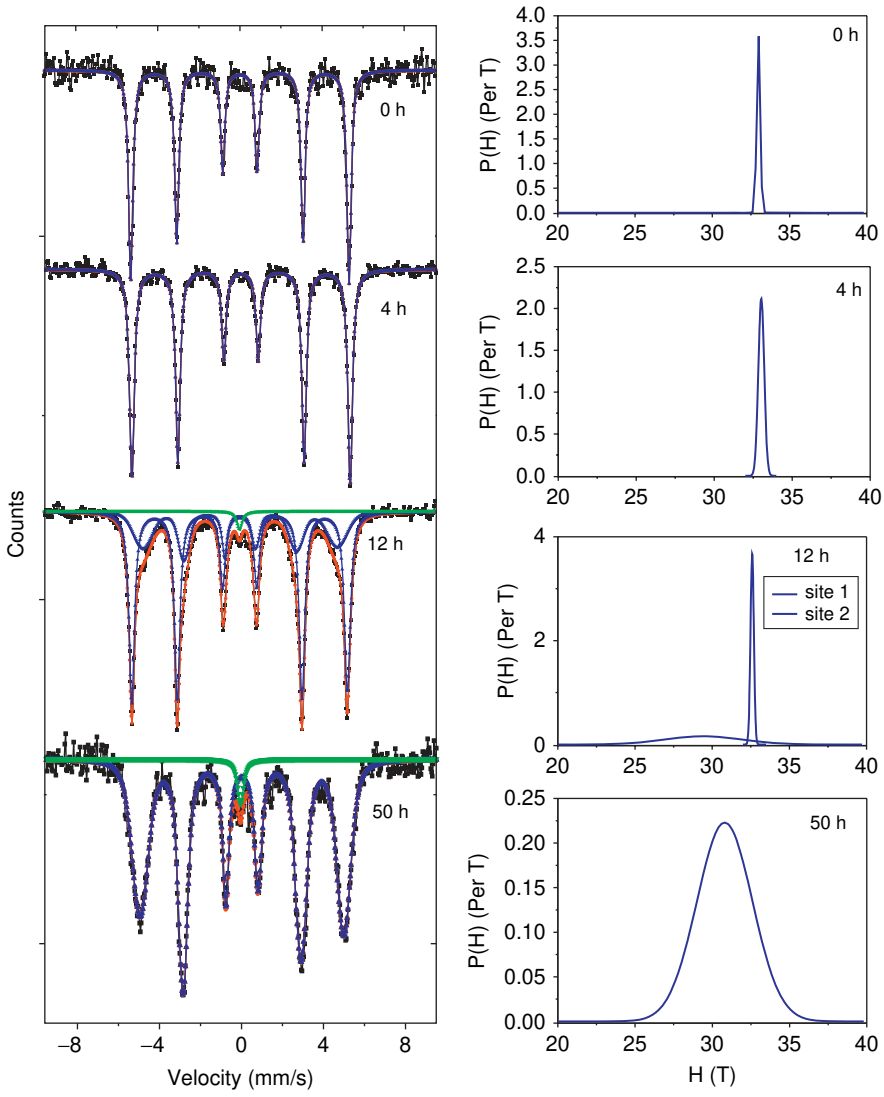

Fig. 6. Room temperature Mössbauer spectra of $Fe_{50}Ni_{50}$ for various milling times and their corresponding hyperfine field distribution obtained from the fitting of the spectra.

and Yang et al. [30]. This has been also observed by Djekoun et al. [23] for mechanical alloyed $Fe_{50}Ni_{50}$. Very similar values of average hyperfine magnetic field were found by Jartych et al. [31] for the final product of $Fe_{50}Ni_{50}$ obtained after 20 h of milling ($\langle H_{hf} \rangle = 30.5$ T) in a high-energy ball milling (Fritsh P5) in which the speed of rotation of mill was 300 rpm, and by Lima et al. [25] ($\langle H_{hf} \rangle = 29.5$ T) for $Fe_{50}Ni_{50}$ nanostructured alloy prepared by chemical reduction. The fact that the hyperfine field values found here for the samples milled at 8 and 12 h (i.e., 30.5 and 29.4 T) are similar to those found for $Fe_{50}Ni_{50}$ as stated above led us to believe that the alloy with composition 50% Fe, 50% Ni starts to form already at 8 h milling time and increases in size with milling time as can be inferred from the increase of the peak intensity from 26.1% for 8 h to 32.7% at 12 h.

For samples milled at 24, 32 and 50 h, the Mössbauer spectra show a six line magnetic spectrum according to their ferromagnetic character, with a broad HFD, according to the disordered character of the alloys. We note also the presence of a singlet line for these samples. The HMHW of sextet lines are equal to 0.158, 0.175 and 0.183 mm/s for 24, 32 and 50 h, respectively. For these samples, the Mössbauer spectra were fitted by one sextet and a singlet line. For the sextets, the mean hyperfine magnetic field values are equal to 30.81(36), 30.805(31) and 30.8 T for 24, 32 and 50 h, respectively. The sextet is attributed to the disordered taenite with $Fe_{50}Ni_{50}$ composition as was pointed by Abdul et al. [32] in mechanical alloying FeNi and the singlet line to the rich fcc iron rich paramagnetic phase [25]. Our results are not far from those found by Jartych et al. [17] where $\langle H_{hf} \rangle$ was equal to 31.5 T for 50 h high-energy ball milled $Fe_{50}Ni_{50}$ and Ping et al. [33] who found a $\langle H_{hf} \rangle$ value of 31 T for splat quenched $Fe_{50}Ni_{50}$ alloy. Also, Cruz et al. [34] found a $\langle H_{hf} \rangle$ value equal to 30.8 T for arc melted $Fe_{50}Ni_{50}$ alloy and Baldokhin et al. [19,35] found a $\langle H_{hf} \rangle$ of 30.8 and 31 T for $Fe_{50}Ni_{50}$ alloy elaborated by gas evaporation

technique and mechanical alloying, respectively. We can also note that for milling times greater than 24 h, the whole amount of iron has reacted with the Ni (absence of pure Fe sextet in the Mössbauer spectra), this results are in agreement with those found by XRD experiments (see Section 3.1) and elemental mapping by EDX (Section 3.2).

3.4. The magnetization curves

In Fig. 7, we show examples of hysteresis curves (magnetization vs applied field H) for samples milled at 2 and 50 h. From these curves, we have deduced the saturation magnetization M_S and the coercive field H_C.

In Fig. 8, we plot M_S as a function of milling time. We can see that there is an overall decrease of M_S from 180 to 133 emu/g as the milling time is increased from 0 to 50 h. Note also that the first decrease in M_S occurs between 0 and 12 h milling time, in this range there is a progressive disappearance of pure Fe and the formation of the alloy, then the M_S value increases slightly at 24 h (recall that at this time, the powder is completely transformed into the FeNi alloy). Further milling of the alloy leads to another decrease in the M_S value. It is interesting to note that both increasing and decreasing M_S with milling time were reported [24]. The different magnetization behavior seems to be related to different mechanisms responsible for the magnetization value such as oxidation, segregation at the grain boundaries, disorder, etc. Note that in our case, oxidation has to be ruled out, since no oxygen contamination was detected by EDAX (see Section 3.2).

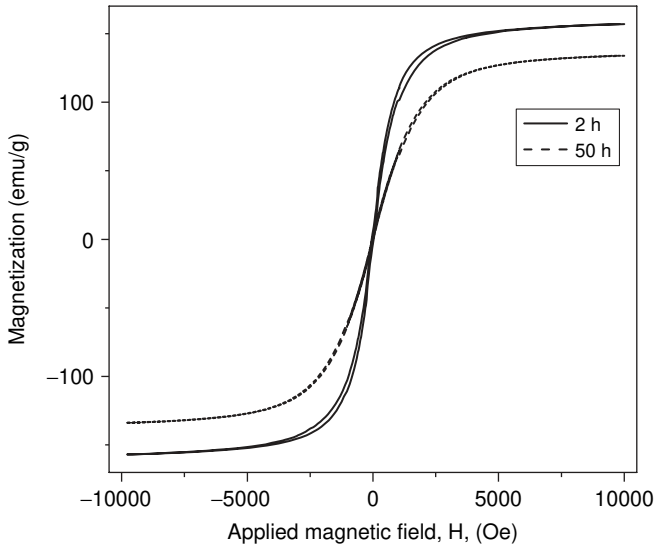

Fig. 7. Hysteresis curves (magnetization vs applied field H) for samples milled at 2 and 50 h.

In Fig. 9, we show the coercive field value as function of milling time t. We can see, from the H_C vs t curve, that in the first region of the curve (between 0 and 4 h), the coercive field is somewhat high, in this range Fe and Ni are still separate elements. Then we note a sharp decrease in H_C, from 36.4 Oe at 4 h to 4 Oe at 8 h milling times; recall that at 8 h, the alloy starts to form. Then H_C monotonously increases from 4 to 19.3 Oe when the milling time increases from 8 to 50 h, i.e, during the formation of the alloy (8–24 h) and when only the phase $Fe_{50}Ni_{50}$ exists (24–50 h). We believe that the increase in H_C with milling time is due to the increase of the strain, recall that strain increases with milling time (see Fig. 3). Indeed, strain through inverse magnetostriction (magneto-elastic effects) may induce an anisotropy which contributes to the value of the coercivity. In fact, many authors have discussed this effect [22,36,37], i.e., that internal strain can be the dominating factor in the coercivity which leads to an increase of H_C with milling time, rather than the usual effect of grain size reduction where it is found that H_C decreases with decreasing grain size (thus with increasing milling time).

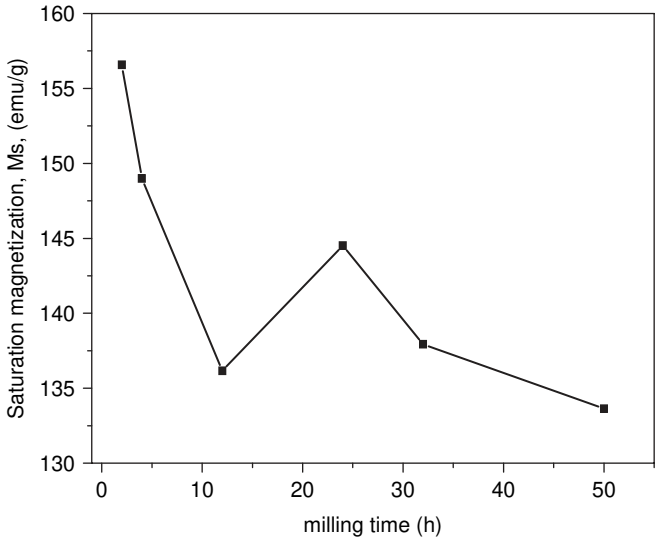

Fig. 8. Saturation magnetization vs milling time.

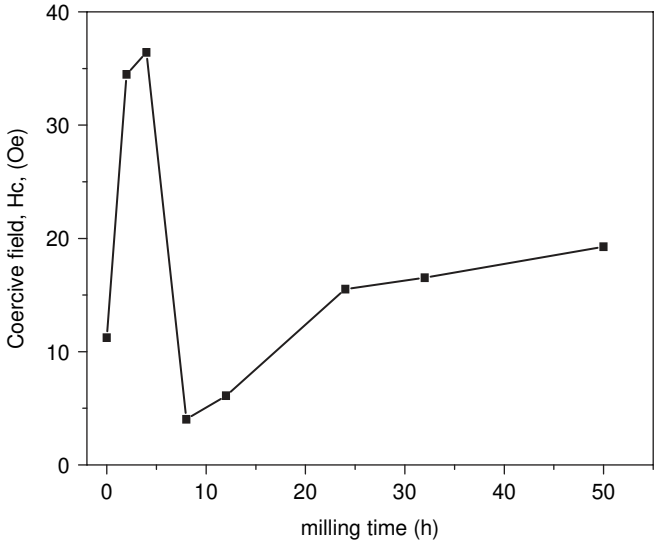

Fig. 9. Coercive field vs milling time.

4. Conclusion

From XRD spectra, we have followed the formation of $Fe_{50}Ni_{50}$ alloy from elemental Fe and Ni powder. It is found that after 8 h milling, the $Fe_{50}Ni_{50}$ starts to form; between 8 and 24 h there is a coexistence of the alloy phase and pure Fe; beyond 24 h all the Fe atoms are dissolved and the powder is completely transformed into the alloy phase. This observation is confirmed by the EDX elemental mapping. Also, the interpretation of the Mössbauer spectra corroborated the fact that $Fe_{50}Ni_{50}$ starts to form after 8 h milling time and that after 24 h there is only the alloy phase. The SEM images taken at different milling time allowed us to follow the morphology of the materials at different stages. Increasing milling time led to an increase of the lattice parameter and the strain values and a decrease of the grain size. The saturation magnetization is found to decrease with increasing milling time. The coercive field H_C increases with increasing milling time, in the milling time range where the alloy starts to form; we believe that magneto-elastic effect is the predominant factor in the coercivity values.

References

[1] S.C. Tjong, H. Chen, Mater. Sci. Eng. R 45 (2004) 1.
[2] C. Kuhrt, L. Schultz, J. Appl. Phys. 71 (1992) 1896.
[3] M.E. McHenry, M.A. Willard, D.E. Laughlin, Prog. Mater. Sci. 44 (1999) 291.
[4] M. Pekala, D. Oleszak, E. Jartych, J.K. Zurawicz, J. Non-Cryst. Solids 250–252 (1999) 757.
[5] Y.V. Baldokhin, P.Y. Kolotyrkin, Y.I. Petrov, E.A. Shafranovsky, Phys. Lett. A 189 (1994) 137.
[6] R.H. Yu, L. Ren, S. Basu, K.M. Unruh, A. Parvizi-Majidi, J.Q. Xiao, J. Appl. Phys. 87 (9) (1999) 5840.
[7] A. Djekoun, B. Bouzabata, S. Alleg, J.M. Greneche, A. Otmani, Ann. Chim. Sci. Mater. 23 (4) (1998) 557.
[8] J.J. Sunol, A. Gonzalez, L. Escoda, J. Mater. Sci. 39 (2004) 5147.
[9] X.G. Li, A. Chiba, S. Takahashi, J. Magn. Magn. Mater. 170 (1997) 339.
[10] C. Suryanarayana, Bull. Mater. Sci. 17 (4) (1994) 307.
[11] C. Suryanarayana, Prog. Mater. Sci. 46 (2001) 1.
[12] V.V. Tcherdyntsev, S.D. Kaloshkin, I.A. Tomilin, E.V. Shelekov, Yu.V. Baldokhin, Nanostruct. Mater. 12 (1999) 139.
[13] S. Krum, WinFit Software, Institut für Geologie, Erlangen, Germany, 1997.
[14] B.E. Warren, B.L. Averbach, J. Appl. Phys. 21 (1950) 595.
[15] K. Lagarek, D. Rancourt, Recoil Software, Physics Department, University of Ottawa, 1998.
[16] L. Castex, J.L. Lebrun, G. Maeder, J.M. Sprauel, Détermination de contraintes résiduelles par diffraction des rayons X, vol. 22, Publications scientifiques et techniques de l'ENSAM, Paris, 1981, pp. 51–60.
[17] E. Jartych, J.K. Zurawicz, D. Oleszak, M. Pękala, Nanostruct. Mater. 12 (1999) 927.
[18] S.D. Kaloshkin, V.V. Tcherdyntsev, I.A. Tomilin, Yu.V. Baldokhin, E.V. Shelekhov, Physica B 229 (2001) 236.
[19] Yu.V. Baldokhin, V.V. Tcherdyntsev, S.D. Khaloshkin, G.A. Kochetov, Yu. A. Pustov, J. Magn. Magn. Mater. 203 (1999) 313.
[20] D. Oleszak, P.H. Shingu, Mater. Sci. Eng. A 181–182 (1994) 1217.
[21] A. Djekoun, A. Otmani, B. Bouzabata, L. Bechiri, N. Randrianantoandro, J.M. Greneche, Catal. Today 113 (2006) 235.
[22] R. Hamzaoui, O. Elkedim, N. Fenineche, E. Gaffet, J. Craven, Mater. Sci. Eng. A 360 (2003) 299.
[23] A. Djekoun, B. Bouzabata, A. Otmani, J.M. Greneche, Catal. Today 89 (2004) 319.
[24] M. Pękala, D. Oleszak, E. Jartych, J.K. Żurawicz, Nanostruct. Mater. 11 (6) (1999) 789.
[25] E. Lima Jr., V. Drago, R. Bolsoni, P.F.P. Fichtner, Solid State Commun. 125 (2003) 265.
[26] R.M. Davis, B. Mc Dermont, C.C. Koch, Met. Trans. 19A (1988) 28.
[27] A. Otmani, B. Bouzabata, A. Djekoun, S. Alleg, Ann. Chim. Sci. Mater. 22 (1997) 201.
[28] E. Lima Jr., V. Drago, J.C. de Lima, P.F.P. Fichtner, J. Alloys Compd. 396 (2005) 10.
[29] R.B. Scorzelli, J. Danon, Phys. Scripta. 32 (1985) 143.
[30] C.W. Yang, D.B. Williams, J.I. Goldstein, J. Phase Equil. 17 (1996) 522.
[31] E. Jartych, J.K. Zurawicz, D. Oleszak, M. Pekala, J. Magn. Magn. Mater. 208 (2000) 221.
[32] Y.A. Abdul, H. Annersten, T. Ericsson, P. Nordblad, J. Magn. Magn. Mater. 280 (2004) 243.
[33] J.Y. Ping, D.G. Rancourt, L.A. Dunlap, J. Magn. Magn. Mater. 103 (1992) 285.
[34] B. Cruz, J.A. Tabares, A. Bohorquez, G.A. Perez Alcazar, Hyperfine Interact. 110 (1997) 7.
[35] Yu.V. Balokhin, P. Ya. Kolotyrkin, Yu.I. Petrov, E.A. Shafranovsky, J. Appl. Phys. 78 (10) (1994) 6496.
[36] R. Hamzaoui, O. Elkedim, E. Gaffet, J.M. Greneche, J. Alloys Compd. 417 (2006) 32.
[37] C. Kuhrt, L. Schultz, J. Appl. Phys. 73 (1993) 6588.